ELSEVIER

Materials Science and Engineering A282 (2000) 109–114

MATERIALS SCIENCE & ENGINEERING A

www.elsevier.com/locate/msea

High-temperature properties of liquid-phase-sintered α-SiC

Robert P. Jensen [a,1], William E. Luecke [b,*], Nitin P. Padture [a], Sheldon M. Wiederhorn [b]

[a] *Department of Metallurgy and Materials Engineering, Institute of Materials Science, University of Connecticut, Storrs, CT 06269, USA*
[b] *Ceramics Division and Materials Science and Engineering Laboratory, National Institute of Standards and Technology, Gaithersburg, MD 20899, USA*

Received 13 September 1999; received in revised form 12 November 1999

Abstract

We have characterized the high-temperature subcritical crack growth and oxidation resistance of a liquid-phase-sintered (LPS) SiC with 20% volume fraction yttrium aluminum garnet (YAG) second phase. Constant stress-rate testing in air in the temperature range 1100–1300°C yielded a crack growth exponent, $n = 38.9 \pm 9.9$ and an activation energy, $Q_{scg} = (380 \pm 237)$ kJ mol^{-1}. Oxidation followed parabolic kinetics in the temperature range 1100–1300°C with an activation energy, $Q_{ox} = (246 \pm 33)$ kJ mol^{-1}. At 1350°C reaction between the growing oxide layer and the YAG second phase produced a low-melting eutectic, resulting in accelerated oxidation. Below 1100°C, oxidation rates were also anomalously high for reasons we do not understand. In the intermediate temperature range, both the oxidation and subcritical crack growth resistance compare favorably with other silicon carbides. Published by Elsevier Science S.A.

Keywords: Silicon carbide; Dynamic fatigue; Constant stress-rate testing; Subcritical crack growth; Oxidation

1. Introduction

There has been growing interest in pressureless liquid-phase sintering (LPS) of SiC, with Al_2O_3 additions [1] or simultaneous Al_2O_3 and Y_2O_3 (or other rare earth oxide) additions [2–5], as it allows sintering at lower temperatures (1850–1900°C) than solid-state sintering (2000–2200°C). Densities in excess of 99% of the theoretical limit can be easily achieved by carefully choosing the composition of the liquid phase and the packing-powder configuration [6,7]. A particularly important aspect of this class of materials is that they can be significantly toughened through careful microstructure design, wherein elongated SiC grain-reinforcements are grown in situ during sintering [8–10]. The elongated nature of the SiC grains and the weakness at the grain boundaries promote crack-wake bridging in these ceramics, resulting in a significant increase in the toughness [8–10]. Liquid-phase-sintered SiC may also be used for elevated-temperature applications. Keppler et al. [11] reported that the strength of LPS SiC fabricated with Y_2O_3 and A1N begins to drop at 1000°C, but very little other high-temperature mechanical properties data exist. With the exception of work by Liu [12], the oxidation behavior of LPS SiC has not been studied either. The objective of this study was to evaluate and understand the high-temperature mechanical properties and oxidation behavior of a LPS SiC ceramic fabricated in-house.

Preliminary tensile creep experiments revealed that the LPS SiC of this study is highly creep-resistant. For instance, in air at 1300°C and 150 MPa, this LPS SiC crept to less than 0.05% strain in 480 h before failing. Fractography indicated that subcritical crack growth was responsible for the failure. Because of the importance of crack growth in failure, this mechanical properties work focusses on studying the effect of stressing rate on the strength (dynamic fatigue) of this ceramic at high-temperatures.

* Corresponding author. Tel.: +1-301-9755744; fax: +1-301-9755334.
E-mail address: william.luecke@nist.gov (W.E. Luecke)
[1] Present address: Caterpillar Corporation Peoria, IL, USA.

0921-5093/00/$ - see front matter Published by Elsevier Science S.A.
PII: S0921-5093(99)00769-8

2. Experimental procedure

2.1. Material

A 99% dense LPS SiC, containing 20% by volume yttrium aluminum garnet (YAG) second phase, was fabricated in our laboratories, using a processing procedure described elsewhere [6–8]. This ceramic contains fine, equiaxed α-SiC grains of average size 1.0 μm; Fig. 2(A) of Ref. [7] shows the microstructure. Characterizing a fine-grained LPS SiC establishes a reference baseline for the high-temperature properties of LPS SiC in general.

2.2. Constant stress-rate testing

Four-point bend specimens ($2 \times 1.5 \times 25$ mm) were machined in-house according to the procedure outlined in the ASTM standard for high-temperature flexural strength [13]. Because of the low Weibull modulus of the as-fabricated material, the specimens were indented using a Knoop diamond pyramid at a load of 98 N. This indentation flaw was oriented perpendicular to the long axis of the specimen. To faciliate the examination of the pre-cracks, the indentation was offset 0.5° from vertical, following the indentation procedure (Section A3.3) for the surface crack in flexure (SCF) method of the ASTM provisional standard for fracture toughness of advanced ceramics [14]. After indenting, the surface residual stress from the indent was eliminated by removing a layer of 4.5 times the depth of the indentation hardness impression by polishing. Strength results in constant stress-rate tests were reproducible only when the indented face was the one that originally faced the interior of the billet. Even with this approach, a number of specimens did not fail from the indentation, and were not included in the analysis.

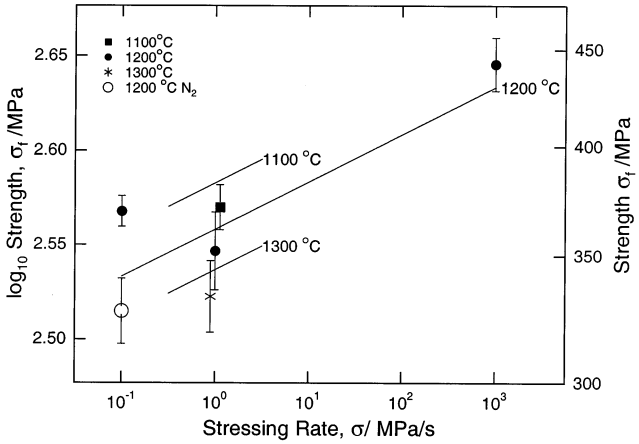

Fig. 1. Strength a function of stressing rate for LPS SiC specimens with 98 N Knoop indentations. Error bars represent the estimated uncertainty of the mean strength. The symbols for the 1 MPa s^{-1} stressing rate have been displaced slightly for clarity. The solid lines are the fit of the natural log of Eq. (2) with parameters $n = (38.9 \pm 9.9)$, $Q_{scg} = (380 \pm 237)$ kJ mol^{-1}, and $\log_e D_0/(n+1) = (5.11 \pm 0.45)$ where D_0 has units to give strengths in MPa when stressing rates are in MPa s^{-1}.

Table 1
Constant stress-rate strength data displayed in Fig. 1

T (°C)	$\dot{\sigma}$ (MPa s^{-1})	Strengths, σ_f (MPa)
Room	80	334, 312, 219
1100	1	391, 387, 354, 353
1200	1000	465, 462, 438, 404
1200	1	388, 366, 358, 356, 293
1200	0.1	382, 381, 358, 357
1300	1	359, 351, 326, 296
Tests conducted in nitrogen		
1200	0.1	356, 339, 322, 296

Constant stress-rate testing of indented specimens in the range 1100–1300°C employed a hot-pressed SiC fixture with 20 mm outer and 10 mm inner spans [15]. Loading rates were 0.01, 1.0, and 1000 MPa s^{-1}. Tests in air employed an electromechanical testing machine (Instron Model 8562, Canton, MA, USA)[2] with SiC push rods in a $MoSi_2$ element furnace. Tests in nitrogen employed a screw-driven testing machine (Instron Model TT, Canton, MA, USA) with the specimen in a sealed $MoSi_2$ element box furnace. All specimens were heated to temperature at 600°C h^{-1} under a 10 N (approximately 33 MPa) preload, soaked for 1 h, and then tested. Specimens tested at 1300°C were soaked for only 10 min. The fracture surfaces were examined with a stereo optical microscope (Leica Wild M10, Heerbrugg Switzerland).

2.3. Oxidation

Specimens for oxidation rate studies were nominally $3 \times 4 \times 10$ mm, although some were slightly wider and shorter. During oxidation in still, room air in a $MoSi_2$ element box furnace, the specimens rested on a sintered SiC plate. At intervals, they were removed from the furnace, weighed to ± 0.0001 g, and returned for further oxidation. Some cross-sections of oxidized specimens were examined using a scanning electron microscope (ESEM2020, Phillips Electron Optics, The Netherlands).

[2] The use of commercial designations or company names is for identification only and does not indicate endorsement by the National Institute of Standards and Technology.

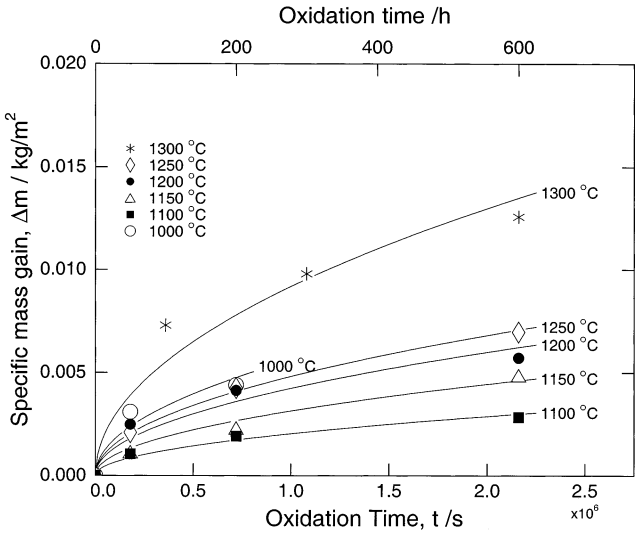

Fig. 2. Specific mass gain as a function of oxidation time. Note that the data for 1000°C lie above much of the higher temperature data. Data for 1350°C lie off-scale. Solid lines are the fits of Eq. (3) to the data.

3. Results

3.1. Evaluation of subcritical crack growth resistance by constant stress-rate testing

Fig. 1 and Table 1 summarize the strengths of the indented specimens. The single open circle in Fig. 1 represents the strength of specimens tested in N_2 gas. The error bars represent the estimated uncertainty of the mean strengths, $s/N^{0.5}$, where s is the estimated standard deviation of the N strength measurements. Note that the mean strength at the lowest stressing rate at 1200°C is substantially higher than the trend from the other two stressing rates.

Although the results of the constant stress-rate tests (Fig. 1) indicate the existence of subcritical crack extension during loading, examination of the fracture surfaces in the optical microscope did not reveal any conclusive evidence of crack extension. In particular, no 'halos' (such as Fig. 9a of Ref. [16]) around the precrack were visible. Frequently, even locating the precrack was difficult.

3.2. Oxidation

Fig. 2 shows the specific mass gain (mass gain per unit area) for specimens oxidized in room air at temperatures between 1000 and 1350°C. Note that the oxidation rate at 1000°C falls above that for 1100–1250°C, a fact that a repeated test (not shown) confirmed. The specific mass gains at 1350°C were substantially higher, and are not plotted. Unlike the specimens oxidized at lower temperatures, which were flat and smooth, the surface of the specimen oxidized at 1350°C was blistered, and the surface oxide had flowed down onto the SiC plate on which the specimen sat.

4. Discussion

4.1. Subcritical crack growth resistance

The resistance to subcritical crack growth in structural ceramics at elevated-temperature is typically evaluated by one of three techniques. Double torsion tests have the advantage that the growing crack is large and easy to follow, but suffer from the disadvantage that the growth of large cracks may not represent the growth of the type of small flaws responsible for failure in service. Constant stress tests (so-called static fatigue or stress rupture) probe the small flaws that are ultimately responsible for failure under service conditions, and have the advantage that they can indicate the propensity for failure from other time-dependent mechanisms besides SCG. Difficulties in interpreting the data if high-temperature exposure generates new flaws and the long testing times are disadvantages. Constant stress-rate testing (dynamic fatigue) allows more more numerous tests and mitigates the contribution of purely time-dependent exposure effects.

Regardless of the test technique, traditionally one assumes that the crack velocity, v, of flaws follows a power law function of the applied stress intensity, K [17,18]:

$$v = v_0 \exp(-Q_{scg}/RT)(K/K_0)^n \quad (1)$$

For extension under constant loading rate, $\dot{\sigma}$, the failure stress, σ_f, has the form [19]:

$$\sigma_f^{n+1} = D_0 \exp\left(\frac{Q_{scg}}{RT}\right)\dot{\sigma} \quad (2)$$

where D_0 is a constant term. Large values of the exponent, n, indicate good resistance to SCG.

Fig. 1 shows the bilinear regression of the natural logarithm of Eq. (2) to the data. This method is the one recommended in ASTM Standard 1368 [20] for determination of subcritical crack growth parameters in structural ceramics at room temperature, although that standard does not employ indented specimens, and folds the activation energy term, Q_{scg}, into the constant, D_0.

The uncertainty in the crack growth exponent, $n(38.9 \pm 9.9)$, comes from the uncertainty in the slope of the $\log \sigma_f - \log \dot{\sigma}$ curve, and arises primarily from the anomalously high mean strength at 1200°C at the lowest loading rate. It is possible that flaw blunting by oxidation during the loading may have caused this increase. The tests in the inert environment, where no such blunting should have occurred, have a much lower strength, (325 ± 11) vs. (369 ± 7) MPa, than those

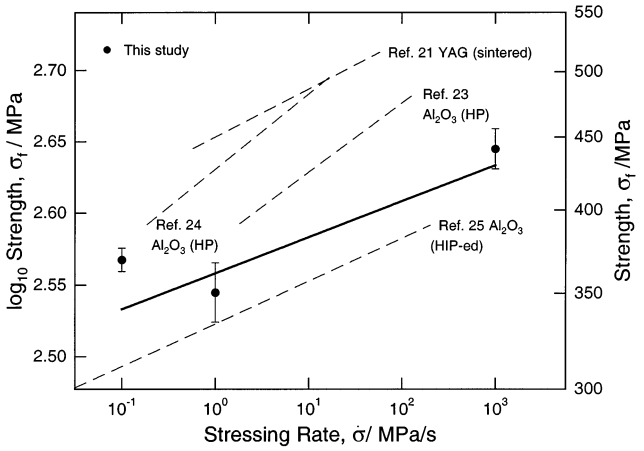

Fig. 3. A comparison of dynamic fatigue data at 1200°C of this LPS SiC with that for SiC hot-pressed with $A1_2O_3$ [22,23] (Norton NC-203) tested in air at 1200°C, SiC HIP-ed with Al [31] tested at 1200°C, and with SiC sintered with Al_2O_3 and Y_2O_3 (Carborundum Hexoloy SX-G1) [21] tested at 1232°C. The absolute values of the strengths are unimportant for comparision. The solid line represents the fit to the full data set of Fig. 1.

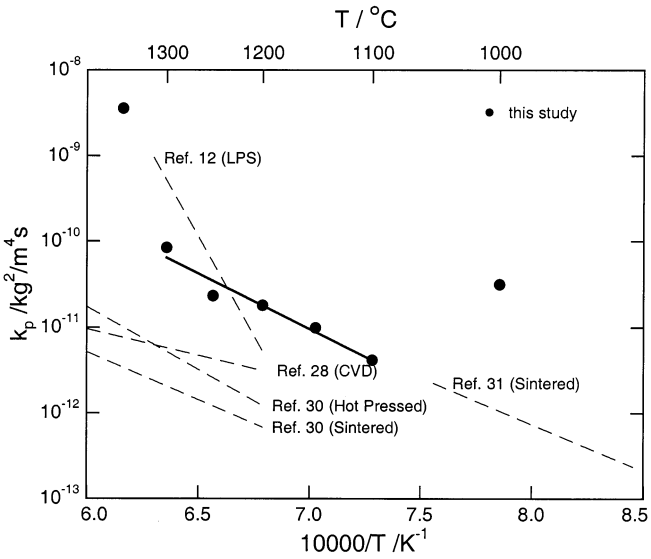

Fig. 4. Parabolic oxidation rate constants for this LPS SiC (filled circles). Data for 1350 and 1000°C have been omitted from the fit. Uncertainties in the k_p are on the order of the size of the symbols. Other data are for SiC hot-pressed with Al_2O_3 (Norton NC-203) [29], a sintered α-SiC (Carborundum) [29], a sintered SiC with 20% mass fraction Y_2O_3 and Al_2O_3 [12], a high-purity chemically vapor deposited SiC [27] oxidized in dry oxygen, and low-temperature oxidation of SiC sintered with boron (Ceradyne Ceralloy 146IG) [30], Where necessary, oxide thicknesses have been converted to specific mass gain constants assuming a density of 2320 kg m^{-3} [32].

tested in air, and lie along the global fit. Specimens in these low stressing rate tests were at temperature for nearly 2 h before failure (1 h soak at no load, plus 1 h to reach the failure load), in contrast to only 1 h total for the specimens at the middle loading rate and 10 min at the highest loading rate.

Fig. 3 and Table 2 compare the data for the results for constant stress-rate tests of this study with those for other silicon carbides densified with oxide additives. None of the materials show a great propensity toward subcritical crack extension: the exponents, n, are all near 20 or greater. The yttria-alumina sintered SiC [21] (designated Hexoloy SX-G1), had a substantially smaller mass fraction of additives (0.02) than the LPS SiC of this study (0.26). Evans et al. [22] and Minford et al. [23] agree well on the properties for $A1_2O_3$ hot-pressed SiC (Norton NC-203). Interestingly, Choi et al. [24] reported the absence of subcritical crack growth ($n = 108$) at 1200°C in the same vintage material, but found $n = 28 \pm 6$ at 1300°C. The SiC of Braue et al. may have a slightly better resistance to SCG than NC-203; one difference is that it was HIP-ed with much less Al_2O_3.

4.2. Oxidation

Typically, oxidation of SiC ceramics, whether sintered or single-crystal, is assumed to be limited by the rate of oxygen transport across the growing silica scale [25–27]. Diffusion-limited reactions such as this give rise to parabolic oxidation kinetics:

$$\Delta m^2 = k_p\, t, \tag{3}$$

where Δm is the specific mass gain (mass gain per unit area) during time, t.

Fig. 2 shows the non-linear least-squares fit of Eq. (3) for the six oxidation conditions. Note that the nature of the fit constrains the lines to pass through the origin. The data at the highest and lowest temperatures deviate strongly from the behavior of the intermediate temperatures, Fig. 4. The oxidation process has an activation

Table 2
A comparison of results from constant stress-rate tests on various silicon carbides densified with oxide additives

Reference	Additive	Q_{scg} KJ mol^{-1}	n	$\mathrm{Log_e}\ D_0/(n+1)$
This study	YAG	380 ± 237	38.9 ± 9.9	5.11 ± 0.45
Chia et al. [21]	YAG (Hexoloy SX-G1)	1130 ± 605	28.7 ± 14.4	3.07 ± 0.67
Evans et al. [22]	Al_2O_3 (NC-203)	689 ± 91	17.9 ± 2.0	3.09 ± 0.21
Minford et al. [23]	Al_2O_3 (NC-203)	806 ± 231	19.6 ± 5.4	2.75 ± 0.35
Braue et al. [31]	Al_2O_3	445 ± 45	32.5 ± 2.4	4.73 ± 0.09

energy, $Q_{ox} = (246 \pm 33)$ kJ mol^{-1}, when data for the highest and lowest temperatures are excluded.

We do not understand the origin of the low-temperature increase in oxidation rate. It is possible that the oxide that forms is not sufficiently deformable to prevent cracking and thus allows ingress of oxygen to the SiC surface. If this is the case, the measured parabolic rate constant is not valid because transport across the growing oxide layer no longer controls the oxidation rate.

At 1350°C, it is likely that the dramatic increase in oxidation rate comes from the reaction between the silica scale formed and the YAG second phase. Bondar' [28] reported that the eutectic in the Y_2O_3–Al_2O_3–SiO_2 system is at 1345°C. Presumably, silica forming by oxidation of silicon carbide reacts with the YAG to form a low viscosity liquid phase, which allows fast transport of oxygen. There was substantial evidence for such a process in the 1350°C oxidation experiments. Fig. 5 shows that the near-surface of the LPS SiC is depleted in the second phase. The existence of this eutectic probably limits the applicability of YAG-sintered SiC to temperatures much below the 1345°C eutectic temperature.

Fig. 4 shows that, in the intermediate temperature range, the oxidation kinetics of this LPS SiC compare favorably with other silicon carbides, despite its much greater fraction of additives. For comparison, Fig. 4 shows data from a SiC hot-pressed with Al_2O_3 (Norton NC-203) [29]; the same grade and vintage of material appears in Fig. 3. There are also data from two silicon carbides sintered with boron [29,30] and a high-purity, chemically vapor deposited SiC [27]. All of these show activation energies comparable to the LPS SiC of this study. Only one material, another LPS SiC [12], sintered with 20% mass fraction YAG, has a very much larger activation energy (880 ± 158 kJ mol^{-1}), which is calculated from directly from the weight-gain data of Fig. 4 of Ref. [12].

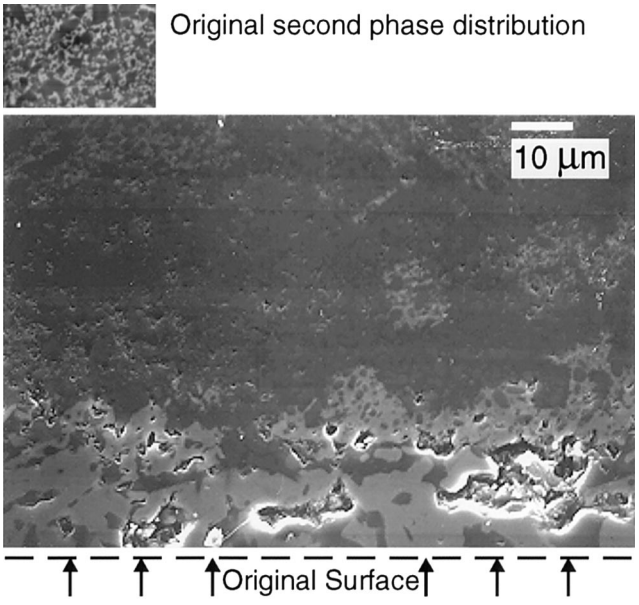

Fig. 5. Scanning electron micrograph of the cross-section of a specimen oxidized 600 h at 1350°C. The oxide layer is enriched in yttrium, and the near-surface is depleted in second phase. The inset shows the second-phase distribution in the starting material at the same magnification.

5. Summary

The resistance to subcritical crack growth at elevated-temperatures of this LPS α-SiC compares favorably with other silicon carbides densified with oxide additives. The oxidation resistance at intermediate temperatures compares favorably with other silicon carbides, but possible reaction by YAG with silica may limit the upper-use temperature to less than 1345°C.

Acknowledgements

The Office of Naval Research supported this work by a grant to the University of Connecticut under the Young Investigator Program (Grant No. N00014-96-1-0654, monitored by Dr S.G. Fishman). We thank Dr V.V. Pujar and Mr G. Quinn for their experimental assistance.

References

[1] K. Suzuki, M. Sasaki, Pressureless sintering of silicon carbide, in: S. Somiya, R.C. Bradt (Eds.), Fundamental Structural Ceramics, Terra Scientific Publishing Company, Tokyo, Japan, 1987, p. 75.
[2] M. Omori, H. Takei, J. Am. Ceram. Soc. 65 (6) (1982) C92.
[3] K. Negita, J. Am. Ceram. Soc. 69 (12) (1986) C308–C310.
[4] L. Cordrey, D.E. Niesz, D.J. Shanefield, Sintering of silicon carbide with rare-earth oxide additions, in: C.A. Handwerker, J.E. Blendell, W.A. Kaysser (Eds.), Sintering of Advanced Ceramics, vol. 7, The American Ceramic Society, Westerville, OH, 1990, p. 618.
[5] M.A. Mulla, V.D. Krstic, Am. Ceram. Soc. Bull. 70 (3) (1991) 439.
[6] V.V. Pujar, R.P. Jensen, N.P., Padture, J. Mater. Sci. Lett. (1999) (in press).
[7] H. Ye, V.V. Pujar, N.P. Padture, Acta Mater. 47 (2) (1999) 481–487.
[8] N.P. Padture, J. Am. Ceram. Soc. 77 (2) (1994) 519–523.
[9] S.K. Lee, Y.C. Kim, C.H. Kim, J. Mater. Sci. 29 (20) (1994) 5321–5326.
[10] M.A. Mulla, V.D. Krstic, Acta Metall. Mater. 42 (1) (1994) 303–308.
[11] M. Keppler, H.-G. Reichert, J.M. Broadley, G. Thurn, I. Wiedmann, F. Aldinger, J. Eur. Ceram. Soc. 18 (1998) 521–526.
[12] D.-M. Liu, Ceram. Int. 23 (1997) 425–436.
[13] Standard test method for flexural strength of advanced ceramics at elevated-temperatures. Standard C1211-98a, American Society for Testing and Materials, West Conshohocken, PA, 1997.

[14] Provisional test methods for determination of fracture toughness of advanced ceramics at ambient temperatures. Provisional Test Method PS 70-97, American Society for Testing and Materials, 1997.
[15] G.D. Quinn, High-temperature flexure fixture for advanced ceramics. Technical Report NISTIR 4864, National Institute of Standards and Technology, Gaithersburg, MD, June 1992.
[16] R.K. Govila, J. Mater. Sci. 19 (1984) 2111–2120.
[17] R.J. Charles, J. Appl. Phys. 29 (12) (1958) 1657–1662.
[18] A.G. Evans, L.R. Russell, D.W. Richerson, Metall. Trans. A 6A (1975) 707–716.
[19] A.G. Evans, Intl. J. Fracture. 10 (2) (1974) 251–259.
[20] Test method for determination of slow crack growth parameters of advanced ceramics by constant stress-rate flexural testing at ambient temperatures. Standard C1369-97, American Society for Testing and Materials, 1997.
[21] K.Y. Chia, S.K. Lau, Ceram. Eng. Sci. Proc. 12 (9-10) (1991) 1845–1861.
[22] A.G. Evans, F.F. Lange, J. Mater. Sci. 10 (1975) 1659–1664.
[23] E. Minford, J.A. Costello, I.S.T. Tsong, R.E. Tressle, Oxidation effects on crack growth and blunting in SiC ceramics, in: R.C. Bradt, A.G. Evans, D.P.H. Hasselman, F.F. Lange (Eds.), Measurements, Transformations, and High-Temperature Fracture, vol. 6 of Fracture Mechanics of Ceramics, Plenum Press, New York, 1983, pp. 511–522.
[24] S.R. Choi, J.A. Salem, N.N. Nemeth, J. Mater. Sci. 33 (1998) 1325–1332.
[25] N.S. Jacobson, E.J. Opila, D.S. Fox, J.L. Smialek, Mater. Sci. Forum 251-254 (1997) 817–832.
[26] E.J. Opila, N.S. Jacobson, Corrosion of ceramic materials, in: M. Schütze (Ed.), Corrosion and Environmental Degradation, vol. 19 of Materials Science and Technology. Wiley-VCH, Weinheim, Germany, 1999.
[27] L.U.J.T. Ogbuji, E.J. Opila, J. Electrochem. Soc. 142 (3) (1995) 925–930.
[28] I.A. Bondar', F.Ya Galakhov. Bulletin of the Academy of Sciences, USSR Division of Chemical Science, 7 (1964) 1231–1232, Translated from Izvestiya Akademii Nauk SSSR, Seriya Khimicheskaya No. 7 July, 1964, 1325–1326.
[29] J.A. Costello, R.E. Tressler, J. Am. Ceram. Soc. 64 (1981) 327–331.
[30] W.E. Luecke, D.L. Kohlstedt, J. Mater. Sci. 25 (1990) 5118–5214.
[31] W. Braue, J. Göring, G. Ziegler, Correlation of subcritical crack growth and microstructure in HIP-SiC, in: V.J. Tennery (Ed.), Third International Symposium on Ceramic Materials and Components for Engines, The American Ceramic Society, Westerville, OH, 1989, pp. 817–830.
[32] K. Luthra, J. Am. Ceram. Soc. 74 (5) (1991) 1095–1103.